Table 2. Ictal video EEG findings and seizure classification

No.	Recording age/onset age (year)	Szs (n)	Video findings: Precipitator	Video findings: Seizure semiology	EEG findings	Seizure classification
2	10/6	3	—	Brief LOC with generalized myoclonus	Diffuse irregular SPW burst	AA
	15/6	1	—	Head and eyes version to Lt followed by Lt arm clonus, which evolved to symmetrical GTC	Rt O predominant recruiting rhythm → diffuse SPW burst	pGTC
3	14/6	2	Watching TV	Repetitive face and upper limbs myoclonus culminating in generalized clonic–tonic–clonic convulsion with eye deviation to Rt	Muscle artifact followed by diffuse slow wave burst with spikes → diffuse rhythmic α → brief SPW burst	GTCS
4	9/6	1	—	Brief LOC	Diffuse irregular SPW burst	AA
	11/6	1	Watching TV	Segmental myoclonus	Bil O dominant diffuse irregular SPW	GMS
	14/6	1	PS	Repetitive upper limbs myoclonus culminating in systemic clonic–tonic–clonic convulsion. Prolonged postictal confusion	Muscle artifact followed by diffuse low voltage α activity → diffuse SPW burst	GTCS
5	7, 8/6	3	Watching TV	Head and eyes version to Lt. Clinging to his mother. Then LOC with eyelids and head clonus, evolved to GTC at once	R pT-O repetitive spikes burst → diffuse SPW burst → Rt O dominant spike burst	CPS or pGTC
	8/6	4	Watching TV	Brief LOC with or without falling backward	Diffuse irregular SPW burst	AA
	8/6	3	Watching TV	Generalized myoclonus, sometimes followed by falling backward	Irregular diffuse SPW	GMS
6	24/6	1	—	Head and eyes version to Lt followed by version to Rt and Rt arm clonus, which evolved to GTC. Prolonged postictal confusion	Rt F-Fz predominant rhythmic θ or Lt C-Cz predominant recruiting rhythm → diffuse rhythmic α → diffuse SPW burst	pGTC
7	11/6	1	—	Head and body version to Lt, followed by automatism of lower limbs with impairment of consciousness	Rt O predominant repetitive spike burst	Partial seizure with automatism
	11/6	1	—	Head and the body version to Rt with Lt arm clonus, which evolved to asymmetrical GTC	Lt O predominant recruiting rhythm → diffuse SPW burst	pGTC
	11/6	2	—	Brief LOC	Diffuse irregular SPW burst	AA
8	25/7	1	PS	Repetitive systemic myoclonus culminating in clonic–tonic–clonic convulsion	Muscle artifact followed by diffuse low voltage α activity → diffuse SPW burst	GTCS
9	17/8	1	PS	The head and body version to Rt, followed by symmetrical GTC	Lt pT-O predominant repetitive spikes burst → diffuse SPW burst	pGTC
12	18/10	1	—	Generalized myoclonus	Irregular diffuse SPW	GMS
13	19/11	2	PS	Generalized myoclonus	Irregular diffuse SPW	GMS
15	24/13	1	—	Brief LOC	2–3 Hz frontal dominant diffuse SPW burst	AA
	24/13	1	Tap sound	Repetitive upper limbs myoclonus culminating in asymmetrical clonic–tonic–clonic seizure with eyes deviation to Rt	Muscle artifact followed by diffuse low voltage α activity → diffuse SPW burst	GTCS
16	31, 44/18	2	Cough (at once)	Head and body version to Rt, followed by asymmetrical tonic posturing with LOC	Lt F-T predominant rhythmic δ → diffuse rhythmic α activity	Partial seizure with tonic posturing

No., patient number; Szs (n), number of seizures; LOC, loss of consciousness; SPW, spike and slow-wave complex; AA, atypical absence seizure; GTCS, generalized tonic–clonic seizure; pGTC, partial seizure evolved GTC; GMS, generalized myoclonic seizure; Bil, bilateral; PS, photostimulation; O, occipital; pT, posterior temporal; F, frontal; Fz, midfrontal; T, temporal; C, central; Cz, midcentral; Lt, left; Rt, right.

Epilepsia, 49(12):2041–2049, 2008
doi: 10.1111/j.1528-1167.2008.01701.x

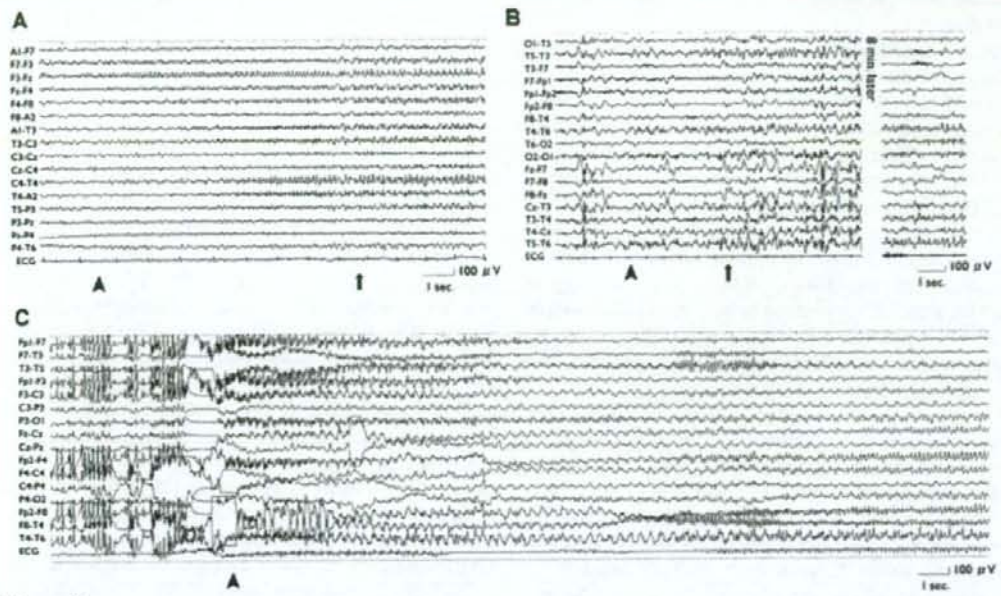

Figure 2.
Representative ictal EEG findings. (**A**) Partial seizure evolved to generalized tonic–clonic convulsion in patient 6. C3-Cz-dominant low voltage fast activity (arrowhead) preceded clinical onset (black arrow) for 10 s. Seizure began with the eye deviated to the left and twitching of the left corner of the mouth, which evolved to generalized tonic–clonic seizure later. (**B**) Complex partial seizure in patient 4. During watching TV, the patient's motion was arrested, and the eyes and head began to verse to the left (arrow). The right posterior temporal-occipital (pT-O) dominant irregular spike burst appeared preceding the clinical onset (arrowhead). Impairment of consciousness continued over 10 min from onset. The patient looked dazzled and often scratched the eyes. In EEG, the spike burst persisted in the right pT-O dominant. (**C**) Generalized clonic–tonic–clonic seizure in patient 3. Repetitive irregular myoclonus was followed by clonic–tonic–clonic seizure (arrowhead). The initial clonic phase was associated with diffuse slow wave burst with spikes in EEG, which evolved to tonic phase with low voltage fast activity in corresponding EEG.

provoked by visual stimulation or cough, but the other six seizures, including five nocturnal seizures, occurred without any precipitating factors. On ictal EEG, focal rhythmic activity (Fig. 2A) or repetitive spike bursts (Fig. 2B) were observed as the initial ictal activity in all seizures. Four of 11 seizures were of frontal origin, while the other seven seizures were of occipital origin. Two patients (patients 6 and 7) had multiple ictal foci (bilateral frontal lobes in patient 6 and bilateral occipital lobes in patient 7).

GTCS (including clonic–tonic–clonic seizures)

Five EEG recordings of GTCS were obtained from four patients. All GTCSs occurred following repetitive trains of stimulus-sensitive myoclonus and culminated in tonic–clonic seizures. On the ictal EEG of three patients, only myogenic artifacts were observed in association with the preceding myoclonus, and then diffuse low voltage fast activity appeared corresponding to the tonic phase, followed by a spike with a slow wave burst corresponding to the clonic phase. In patient 3, an initial clonic phase preceding the tonic–clonic phase was observed, accompanying a diffuse spike with slow wave burst (Fig. 2C).

Prolonged postictal confusion was recorded in two seizures (after pGTC in patient 6 and GTCS in patient 4), both of which continued for over 30 min. We analyzed the interval between epilepsy onset and ictal recording of the three seizure subtypes. Brief generalized seizures were recorded mainly in the early stage (usually less than 8 years from epilepsy onset). In contrast, GTCS were recorded in the progressed stage. All five GTCS were recorded in patients more than 8 years from epilepsy onset, who were almost bedridden. Partial seizures were recorded in every stage throughout the clinical course.

Characteristics of epileptic seizures evaluated from interviews

Seizure semiology other than that of myoclonic seizure is shown in Table 3. Myoclonic seizure was not included in this evaluation, because it could not be distinguished from nonepileptic myoclonus based on the information obtained at interviews. Evaluation of the interview contents revealed that 13 of 17 patients (76%) probably had seizures with focal features as habitual seizures from the early stage of the disease. The seizure manifestations were reported to be head and eyes version and sometimes turning of the body at the onset of seizure, identical to the seizures recorded on ictal video EEG. They evolved frequently to pGTC with or without lateralized symptoms. Impairment of consciousness or automatism without convulsion was observed in a small number of patients.

Six patients (35%) sometimes manifested aura at the onset of the seizure with other focal features. Four of six patients had visual aura as indicated by, for example, exclaiming "Insect! Insect!" or saying that "something is moving." The other two patients just clung to or called for their mothers around the onset of seizure. These auras disappeared within 5 years from epilepsy onset in all patients. As an aura is generally regarded as the most reliable feature for partial seizure (van Donselaar et al., 1990), we defined those patients manifesting an aura and/or having partial seizures confirmed by video EEG recordings as patients with "definitive partial seizure." The number of patients with definitive partial seizure was 11 out of 17 patients (64%).

We compared the age at epilepsy onset, age at clinical onset, and number of CAG repeats between patients having definitive partial seizures (n = 11) and patients without definitive partial seizures (n = 6). The age of epilepsy onset was significantly lower in the group with definitive partial seizures [7.5 ± 3.8 (4–18) years] than in the group without [12.0 ± 3.3 (8–17) years, p = 0.02]. However, patients with and without definitive partial seizures were not significantly different both in age of clinical onset [5.9 ± 4.5 (2–18) years versus 10.8 ± 6.1 (4–18) years, p = 0.06] and the number of CAG repeats [70.0 ± 4.2 (64–76) years versus 69.4 ± 3.1 (65–73) years, p = 0.96]. The prevalence of definitive partial seizures was significantly higher in patients with younger epilepsy onset (below 10 years of age) compared to those with older onset (χ^2 test, $p < 0.05$). The same results were obtained between patients with and without focal feature in their habitual seizures from the interviews (data not shown).

Ictal symptoms suggesting GTCS were described in 13 patients (76%). In six of 13 patients, GTCS were observed subsequent to repetitive myoclonic jerkings. GTCS were usually observed several years after the onset of epilepsy. GTCS were often provoked by some kinds of stimulation, in particular, visual stimulation (71%). Prolonged (about 30 min or longer) postictal confusion after convulsive seizures was experienced by eight patients (47%). Postictal manifestations of excitation, violent behavior, and groaning with confusion were described after convulsive seizures. Postictal confusion continued for 2 h at the longest.

Table 3. Seizure semiology analyzed from interviews and other evaluations

Patient No.	Seizure with focal features			PPIC	Precipitator	PPR	Medications at latest follow-up
	Lateral sign	Aura	Other seizures[a]				
1	Version, focal motor	Visual	GTCS	—	Cough	—	VPA, PHT, ZNS, PB, CZP
2	Version	—	Atonic, GTCS	+	Visual	+	VPA, CZP
3	Version, focal motor	Fear	Absence, GTCS	+	Visual, pain	+	VPA, CZP
4	Version	Visual	Absence, atonic	+	Visual	+	VPA, ZNS, PB, CZP
5	Version, focal motor	—	Absence, atonic, GTCS	+	Visual	+	VPA, ZNS, ESM
6	Version, focal motor	—	—	+	Visual	+	VPA, ZNS, CZP
7	Version	Fear	Absence, atonic	+	Visual	+	VPA, ZNS, CZP
8	Version	Visual	—	—	Visual	—	VPA, ZNS, CZP
9	Version	—	GTCS	+	Visual	+	VPA, PHT, CLB
10	Version	—	GTCS	—	Visual	+	VPA, ZNS, CZP,
11	—	—	Absence, GTCS	—	—	+	VPA, CZP, CLB
12	Version	Visual	Atonic, GTCS	—	—	+	VPA, CLB
13	—	—	GTCS	—	Visual	+	VPA, PB, ZNS
14	—	—	GTCS	—	—	—	VPA, ZNS, CZP
15	Version	—	GTCS	+	—	+	VPA
16	Version	—	Absence, GTCS	—	Visual, cough	—	VPA, PHT, ZNS, PB, CZP
17	—	—	GTCS	+	—	—	VPA, PB, CZP

No., number; GTCS, generalized tonic–clonic seizure; PPIC, prolonged post ictal confusion; PPR, photoparoxysmal response; VPA, valproic acid; PHT, phenytoin; ZNS, zonisamide; CZP, clonazepam; CLB, clobazam; PB, phenobarbital.

[a]Myoclonic seizure was excluded.

Interictal EEG

Interictal EEG demonstrated unusual background activity of varying degrees in individual patients. In more severely mentally retarded patients with a longer CAG repeat length (patients 2, 3, and 5), the background activity was ambiguous due to prominent paroxysmal discharges overriding diffuse slow waves. In contrast, an occipital-dominant slow α (9–10 Hz) background activity could be clearly distinguished in less mentally retarded patients with a shorter CAG repeat length (patients 1 and 12). Interictal discharges were most frequently observed as diffuse irregular spike-and-wave complexes. Independent occipital or frontal-dominant spikes or spike-and-wave complexes were also observed frequently (88% of patients), but the laterality was not consistent in all patients. PPR was positive in 76% of patients.

In sleep EEG, the usual spindle waves and K-complexes disappeared in all patients. Paroxysmal discharges increased during sleep. Frontal-dominant diffuse spike-and-wave complex bursts or slow wave bursts with or without spikes were observed in 76% of patients. Some patients (18%) present high voltage (over 300 μV) slow wave bursts with bilateral frontal dominance.

Medical treatments

The medications prescribed in our hospital for each patient at the latest follow-up are shown in Table 3. Valproic acid (VPA) was used in all patients. At the time of referral to our hospital, all patients except one had already taken various combinations of antiepileptic drugs. Carbamazepine (CBZ) was administered to eight patients before referral and was withdrawn resulting in no consistent changes of seizures and myoclonus. Similarly, phenytoin (PHT) was discontinued in five out of seven patients administered this drug before referral. In one case (patient 9), PHT was restarted due to seizure aggravation. We never initiated CBZ or PHT or both by ourselves in any of the patients. Although various drug regimens were tried, remarkable and continuous seizure remission was not obtained in all patients.

Discussion

In this study, the electroclinical features of epilepsy in juvenile type DRPLA were studied by ictal video EEG recordings and clinical interviews. We obtained the following findings: (1) frequent association of habitual partial seizures in a large proportion of patients; (2) higher prevalence of partial seizures in patients with younger onset of epilepsy; and (3) evolutional changes of epileptic seizures from brief generalized seizures to GTCS. The value of CAG repeat length in this study (mean ± SD, 69.9 ± 3.7; range, 64–76; n = 17) was no different to those of previous reports evaluating juvenile type DRPLA in larger numbers of patients [median 68.0, range 63–79, n = 24 (Ikeuchi et al., 1995); mean 67.1, n = 20 (Komure et al., 1995)]. As it is well known that the CAG repeat length strongly correlates with clinical severity (Tsuji, 1999), the population in this study can be considered as representative of juvenile type DRPLA.

We were able to confirm frequent association of partial seizures by both ictal video EEG recordings and clinical interviews. Partial seizures were reported in some kinds of PME, such as visual seizures in Lafora's disease (Tinuper et al., 1985), but the presence of partial seizure was reported in only a small number of cases of juvenile type DRPLA. One case report briefly mentioned the presence of complex partial seizure (Saitoh et al., 1998). Another case report described partial seizures along with ictal EEG in a patient with clinical onset below 2 years of age, and proposed that rare cases of juvenile type DRPLA with very early onset might manifest partial seizures (Hattori et al., 1997). In our study, interviews to obtain information related to seizure semiology indicated that over three-fourths of the patients had focal features in their habitual seizures. The features were mainly versive movements, preceded by an aura in almost one-half of the patients. Although ictal symptoms with focal features such as version or asymmetric tonic posturing are sometimes observed in patients with generalized epilepsy (Niaz et al., 1999; Usui et al., 2005), the presence of aura is generally accepted as the most reliable sign of partial seizure (van Donselaar et al., 1990). Accordingly, at least 11 of our 17 patients (64%) had habitual partial seizures, judging from ictal video EEG recordings, or presence of an aura, or both. The prevalence of partial seizures in DRPLA seems to be higher than compared to other PMEs, including Lafora disease (33%–50%) (Acharya et al., 1993; Genton et al., 2005). In our study, approximately two-thirds of partial seizures showed discharges of occipital origin on ictal video EEG recordings, and visual symptom was the main feature of the aura. Occipital seizure may be the most common partial seizure in juvenile type DRPLA, as is also in Lafora disease.

We were able to confirm a higher prevalence of partial seizures in patients with earlier onset of epilepsy. The association of habitual partial seizures was significantly related to the age of epilepsy onset, but not to the number of CAG repeats. Also, our data of ictal video EEG recordings suggested that partial seizures occurred both in early and advanced stages. These data suggest that partial seizures occur in patients with younger epilepsy onset in an age-dependent manner and continue up to advanced stages. Moshé et al. (1995) pointed out that the susceptibility of human brain to focal seizures alters during development, and they documented a continuous increase in susceptibility until the periadolescence stage in mice. They proposed that age-dependent changes in the developing brain such as the synaptic formation, ionic environmental alternation, and myelination may contribute to the semiological alteration. Our result was in line with their arguments, and the

higher prevalence of partial seizures in DRPLA compared to other PMEs may be explained not only by the genetic difference but also by the earlier onset of epilepsy in juvenile type DRPLA. In a report of 23 patients with genetically confirmed Lafora disease (Franceschetti et al., 2006), the onset age [13.7 ± 2.6 years (8.5–18.5)] was older than that of the patients in our study.

From the evaluation of ictal video EEG, GTCS tended to occur in the advanced stages of the disease, when the patients were almost bedridden, and the generalized tonic–clonic convulsions were often of partial origin. As the disease progressed, focal features tended to become less well defined. These findings suggest that GTCS of generalized nature may occur much less commonly than is generally perceived in patients with juvenile type DRPLA (Tsuji, 1999). On the other hand, brief generalized seizures were frequently observed in the early stage and decreased as the disease progressed. These evolutional changes of epileptic seizures are important diagnostic clues of DRPLA. These changes may be causally related to the pathological involvement associated with cumulation of the mutant DRPLA protein, atrophin-1 (Yamada et al., 2001; Sakai et al., 2006). GTCS in the advanced stage might reflect pathological evolution of the whole brain. Prolonged postictal confusion was also one of the characteristic features of epileptic seizures in juvenile type DRPLA. Long-lasting postictal confusion was also reported as one of the characteristic features of the epilepsy in older patients (Cloyd et al., 2006). Therefore, the prolonged postictal confusion may be attributed to the attenuation of cortical functions in DRPLA and may be one of the diagnostic clues in patients with DRPLA.

In this study, we present the characteristics of epileptic seizures in patients with juvenile DRPLA. Recognition of the characteristics would contribute to early diagnosis and proper treatments. As a limitation of this retrospective study, we were not able to illustrate the change of seizure semiology longitudinally in each patient or to propose a potential strategy for medical treatment. As aggravating effects of CBZ and PHT have been shown in other PMEs (Elridge et al., 1983; Corlill & Hredie, 1999), the effects of these antiepileptic agents on juvenile DRPLA are of great interest. From the clinical courses of our patients who had been administered CBZ and PHT at referral, the effects of these drugs seem not to be apparent in juvenile type DRPLA. However, the precise effects remain to be studied. Further prospective studies are required to obtain a deeper understanding about seizure semiology and medication strategies for juvenile type DRPLA.

Acknowledgments

The authors thank Dr. Fumiaki Tanaka at Nagoya University Graduate School of Medicine for DNA analysis. This study was funded in part by Research Grants (19A-6) for Nervous and Mental Disorders from the Ministry of Health, Labor and Welfare, grants-in-aid for Scientific Research I No. 19591234, Health and Labor Sciences Research Grants for Research on Psychiatry and Neurological Diseases and Mental Health (H-017) (H20–021), and grants from The Japan Epilepsy Research Foundation.

Conflict of interest: We confirm that we have read the Journal's position on issues involved in ethical publication and affirm that this report is consistent with those guidelines. The authors declare no conflicts of interest.

References

Acharya JN, Satischandra P, Asha T, Shankar SK. (1993) Lafora's disease in south India: a clinical, electrophysiologic, and pathologic study. *Epilepsia* 34:476–487.

Brunetti-Pierri N, Wilfong AA, Hunter JV, Craigen WJ. (2006) A severe case of dentatorubro-pallidoluysian atrophy (DRPLA) with microcephaly, very early onset of seizures, and cerebral white matter involvement. *Neuropediatrics* 37:308–311.

Cloyd J, Hauser W, Towne A, Ramsay R, Mattson R, Gilliam F, Walczak T. (2006) Epidemiological and medical aspects of epilepsy in the elderly. *Epilepsy Res* 68(Suppl 1):S39–S48.

Corkill RG, Hardie RJ. (1999) An unusual case of Larofa body disease. *Eur J Neurol* 6:245–247.

Elridge R, Iivanainen M, Stern R, Koerber I, Wilder BJ. (1983) 'Baltic' myoclonus epilepsy: hereditary disorder of childhood made worse by phenytoin. *Lancet* 322:838–842.

Franceschetti S, Gambardella A, Canafoglia L, Striano P, Lohi H, Gennaro E, Ianzano L, Veggiotti P, Sofia V, Biondi R, Striano S, Gellera C, Annesi G, Madia F, Civitelli D, Rocca FE, Quattrone A, Avanzini G, Minassian B, Zara F. (2006) Clinical and genetic findings in 26 Italian patients with Lafora disease. *Epilepsia* 47:640–643.

Genton P, Malafosse A, Moulard B. (2005) Progressive myoclonus epilepsies. In Roger J, Bureau M, Dravet Ch, Genton P, Tassinari CA, Wolf P (Eds) *Epileptic syndrome in infancy, childhood and adolescence*. 4th ed. John Libbey Eurotext, Montrouge, pp. 441–466.

Hattori H, Higuchi Y, Okuno T, Asato R, Fukumoto M, Kondo I. (1997) Early-childhood progressive myoclonus epilepsy presenting as partial seizures in dentatorubral-pallidoluysian atrophy. *Epilepsia* 38:271–274.

Ikeuchi T, Koide R, Tanaka H, Onodera O, Igarashi S, Takahashi H, Kondo R, Ishikawa A, Tomoda A, Miike T, Sato K, Ihara Y, Hayabara T, Isa F, Tanabe H, Tokiguchi S, Hayashi M, Shimizu N, Ikuta F, Naito H, Tsuji S. (1995) Dentatorubral-pallidoluysian atrophy: clinical features are closely related to unstable expansions of trinucleotide (CAG) repeat. *Ann Neurol* 37:769–775.

Kasteleijn-Nolst T. (1989) Photosensitivity in epilepsy. Electrophysiological and clinical correlates. *Acta Neurol Scand Suppl* 125:3–149.

Koide R, Ikeuchi T, Onodera O, Tanaka H, Igarashi S, Endo K, Takahashi H, Kondo R, Ishikawa A, Hayashi T, Saito A, Tomoda T, Miike H, Naito H, Ikuta F, Tsuji S. (1994) Unstable expansion of CAG repeat in hereditary dentatorubral-pallidoluysian atrophy (DRPLA). *Nat Genet* 6:9–13.

Komure O, Sano A, Nishino N, Yamauchi N, Ueno S, Kondoh K, Sano N, Takahashi M, Murayama N, Kondo I, Nagafuchi S, Yamada M, Kanazawa I. (1995) DNA analysis in hereditary dentatorubral-pallidoluysian atrophy: correlation between CAG repeat length and phenotypic variation and the molecular basis of anticipation. *Neurology* 45:143–149.

Licht DJ, Lynch DR. (2002) Juvenile dentatorubral-pallidoluysian atrophy: new clinical features. *Pediatr Neurol* 26:51–54.

Moshé SL, Shinnar S, Swann JW. (1995) Partial (focal) seizures in developing brain. In Schwartzkroin PA, Moshé SL, Noebels JL, Swann JW (Eds) *Brain development and epilepsy*. Oxford University Press, New York, pp. 34–65.

Munoz E, Mila M, Sanchez A, Latorre P, Ariza A, Codina M, Ballesta F, Tolosa E. (1999) Dentatorubropallidoluysian atrophy in a Spanish family: a clinical, radiological, pathological, and genetic study. *J Neurol Neurosurg Psychiatry* 67:811–814.

Nagafuchi S, Yanagisawa H, Sato K, Shirayama T, Ohsaki E, Bundo M, Takeda T, Tadokoro K, Kondo I, Murayama N, Tanaka Y, Kikushima H, Umino K, Kurosawa H, Furukawa H, Nihei K, Inoue T, Sano A,

Komure O, Takahashi M, Yoshizawa T, Kanazawa I, Yamada M. (1994) Dentatorubral and pallidoluysian atrophy expansion of an unstable CAG trinucleotide on chromosome 12p. *Nat Genet* 6:14–18.

Naito H, Oyanagi S. (1982) Familial myoclonus epilepsy and choreoathetosis: hereditary dentatorubral-pallidoluysian atrophy. *Neurology* 32:798–807.

Niaz FE, Abou-Khalil B, Fakhoury T. (1999) The generalized tonic–clonic seizure in partial versus generalized epilepsy: semiologic differences. *Epilepsia* 40:1664–1666.

Saitoh S, Momoi MY, Yamagata T, Miyao M, Suwa K. (1998) Clinical and electroencephalographic findings in juvenile type DRPLA. *Pediatr Neurol* 18:265–268.

Sakai K, Yamada M, Sato T, Yamada M, Tsuji S, Takahashi H. (2006) Neuronal atrophy and synaptic alteration in a mouse model of dentatorubral-pallidoluysian atrophy. *Brain* 129:2353–2362.

The Commission on Classification and Terminology of the International League Against Epilepsy. (1981) Proposal for revised clinical and electroencephalographic classification of epileptic seizures. *Epilepsia* 22:489–501.

Tinuper P, Gobbi G, Aguglia U, Rossi PG, Lugaresi E. (1985) Occipital seizures in Lafora disease: a further case documented by EEG. *Clin Electroencephalogr* 16:167–170.

Tsuji S. (1999) Dentatorubral-pallidoluysian atrophy (DRPLA): clinical features and molecular genetics. *Adv Neurol* 79:399–409.

Usui N, Kotagal P, Matsumoto R, Kellinghaus C, Luders HO. (2005) Focal semiologic and electroencephalographic features in patients with juvenile myoclonic epilepsy. *Epilepsia* 46:1668–1676.

van Donselaar CA, Geerts AT, Schimsheimer RJ. (1990) Usefulness of an aura for classification of a first generalized seizure. *Epilepsia* 31:529C535.

Yamada M, Wood JD, Shimohata T, Hayashi S, Tsuji S, Ross CA, Takahashi H. (2001) Widespread occurrence of intranuclear atrophin-1 accumulation in the central nervous system neurons of patients with dentatorubral-pallidoluysian atrophy. *Ann Neurol* 49:14–23.

ELSEVIER

Journal of the Neurological Sciences 269 (2008) 30 – 34

Journal of the Neurological Sciences

www.elsevier.com/locate/jns

Anterior horn cells with abnormal TDP-43 immunoreactivities show fragmentation of the Golgi apparatus in ALS

Yukio Fujita [a,*], Yuji Mizuno [a], Masamitsu Takatama [b], Koichi Okamoto [a]

[a] *Department of Neurology, Gunma University Graduate School of Medicine, Maebashi, Gunma, Japan*
[b] *Geriatric Research Institute and Hospital, Maebashi, Gunma, Japan*

Received 28 November 2007; accepted 11 December 2007
Available online 22 January 2008

Abstract

Recently, TAR DNA-binding protein of 43-kDa (TDP-43) was identified as a major component of ubiquitinated neuronal cytoplasmic inclusions observed in lower motor neurons in amyotrophic lateral sclerosis (ALS) and frontotemporal lobar degeneration with ubiquitinated inclusions. We herein investigated the relationship between TDP-43 immunoreactivities and fragmentation of the Golgi apparatus (GA). Each mirror section of spinal cord tissues in 10 ALS and 3 control cases were immunostained with polyclonal anti-TDP-43 and polyclonal anti-trans-Golgi-network (TGN)-46 antibodies. The neurons were divided into subtypes according to differences in TDP-43 immunoreactivities, and we examined the morphological changes of GA in each type. We divided the neurons into four subtypes according to the observed differences in TDP-43 immunoreactivities, Type A: neurons showing normal nuclear staining, Type B: neurons showing a loss of normal nuclear staining and a few granular cytoplasmic immunoreactivities, Type C: neurons showing a lot of granular immunoreactivities and no inclusions, Type D: neurons with inclusions. All of the neurons in Type A showed normal GA profiles, however, almost all of the neurons with abnormal TDP-43 immunoreactivities (Type B–D) showed GA fragmentation. These results suggest that neurons with abnormal TDP-43 immunoreactivities are associated with dysfunction of the secretory pathway in motor neurons.

Keywords: Amyotrophic lateral sclerosis; TAR DNA-binding protein of 43-kDa (TDP-43); Golgi apparatus; Spinal cord; Cytoplasmic inclusion; Neuropathology

1. Introduction

Amyotrophic lateral sclerosis (ALS) is a chronic degenerative disease characterized by the progressive degeneration and loss of motor neurons in the spinal cord, brainstem, and motor cortex. The etiology of the sporadic form of ALS, representing approximately 90% of all cases, is unknown. The hallmark of neuropathological findings in ALS is significant motor neuron loss, Bunina bodies, and the abnormal accumulation of insoluble ubiquitinated cytoplasmic inclusions in the lower motor neurons, such as skein-like and round inclusions; however, little is known about the specific biochemical composition of these neuronal cytoplasmic inclusions. Recently, the TAR DNA-binding protein of 43kDa (TDP-43), a nuclear protein which is involved in transcriptional repression and alternative splicing, was identified as a major component of neuronal cytoplasmic inclusions in motor neurons in ALS, as well as in frontotemporal lobar degeneration with ubiquitinated inclusions (FTLD-U) [1,2].

Several reports have described that the Golgi apparatus (GA) is frequently fragmented in the anterior horn cells of patients with sporadic ALS; namely, the organelles lose their normal network-like configuration, which is replaced by disconnected small elements [3–10]. Furthermore, the GA of spinal motor neurons was also often fragmented in patients with juvenile ALS with basophilic inclusions [11], and familial ALS with posterior column involvement [12]. Golgi fragmentation was

* Corresponding author. Department of Neurology, Gunma University School of Medicine, 3-39-15, Showa-machi, Maebashi, Gunma 371-8511, Japan. Fax: +81 27 220 8068.
E-mail address: yfujita@showa.gunma-u.ac.jp (Y. Fujita).

0022-510X/$ - see front matter © 2007 Elsevier B.V. All rights reserved.
doi:10.1016/j.jns.2007.12.016

also detected in motor neurons of asymptomatic and paralyzed transgenic mice expressing G93A mutations of SOD1 [13]. So, we considered that the GA is an early target of the pathological processes that initiate neuronal degeneration. We also observed that a majority of motor neurons containing intracytoplasmic inclusions such as Bunina bodies, basophilic inclusions, and SOD1-positive aggregates had fragmented GA [10,11,14]. Therefore, interactions between mutant proteins and any of one or more proteins involved in the maintenance of the structure of the GA might disrupt its structure and function [15].

In this study, we investigated the relationship between TDP-43 immunoreactivities and morphological changes of the GA by immunohistological methods.

2. Materials and methods

Spinal cord tissues of 10 autopsied cases with sporadic ALS and 3 control cases were fixed in phosphate-buffered formalin and embedded in paraffin (Table 1). Three-micrometer-thick deparaffinized mirror sections of the spinal transverse cords were prepared and immunostained with two polyclonal rabbit antibodies against TDP-43 (1:8,000, Protein Tech Group, Inc., Chicago, IL, USA) and human trans-Golgi-network (TGN)-46 (1:4,000). Anti-TGN-46 antibody raised against a synthetic polypeptide, VPLLATESVKQEEAGVRPC (residues 18–35 of human TGN plus a cysteine residue), recognizes an intrinsic membrane protein of the TGN, and this was prepared in our laboratory [16,17]. Autoclave treatment (121 °C, 10 min) was required to improve the antigen, and, after blocking endogenous peroxidase activity in 0.3% H_2O_2 (30 min), the sections were incubated with anti-TGN-46 antibody, and the other mirror sections were incubated with anti-TDP-43 antibody overnight at 4 °C. Incubations with the secondary reagent containing biotinylated anti-rabbit IgG for 30 min, and finally ABC for 30 min, were performed. The tissues were subjected to the peroxidase reaction using the VIP Substrate Kit (Vector) for those with anti-TGN-46 antibody, and diaminobenzidine for those with anti-TDP-43 antibody. Subsequently, the sections were photographed, and those immunostained with anti-TGN-46 antibody were turned upside down. We divided the neurons into subtypes according to differences in TDP-43 immunoreactivities, and examined the morphological changes of the GA in each of these subtypes.

Table 1
Clinical and neuropathological findings of 10 ALS and 3 control cases

Case	Sex	Age at death (years)	Diagnosis	Duration of disease (months)	Respirator (months)	Neuronal inclusions
1	F	56	Sporadic ALS	13	–	BBs, UIs
2	M	60	Sporadic ALS	36	19	BBs, UIs
3	M	62	Sporadic ALS	24	–	BBs, UIs
4	F	64	Sporadic ALS	84	–	BBs, UIs
5	F	69	Sporadic ALS	15	–	BBs, UIs
6	F	70	Sporadic ALS	36	–	BBs, UIs
7	M	75	Sporadic ALS	7	–	BBs, UIs
8	M	75	Sporadic ALS	15	–	BBs, UIs
9	M	79	Sporadic ALS	5	–	BBs, UIs
10	F	81	Sporadic ALS	5	1	BBs, UIs
11	M	34	Liver cirrhosis			
12	F	71	AMI			
13	F	86	Ileus			

M: male, F: female, ALS: amyotrophic lateral sclerosis, BBs: Bunina bodies, UIs: ubiquitinated inclusions, AMI: acute myocardial infarction.

3. Results

In control cases, TDP-43 nuclear stainings were observed in the anterior horn cells of the spinal cord, but no cytoplasmic TDP-43 immunoreactivities were found (Fig. 1a1). On the other hand, in ALS, we observed various abnormal TDP-43 immunoreactivities in the anterior horn cells, and the majority of these neurons showed little or no TDP-43 nuclear staining. We divided these neurons into four subtypes according to differences in TDP-43 immunoreactivities: Type A: neurons showing normal nuclear staining (Fig. 1 b1), Type B: neurons exhibiting a loss of normal nuclear staining and a few fine granular cytoplasmic TDP-43 immunoreactivities (Fig. 1d1, arrow), Type C: neurons showing a lot of granular TDP-43 immunoreactivities and no inclusions (Fig. 1c1), and Type D: neurons with skein-like or round inclusions (Fig. 1d1, arrowhead). We could not detect a relationship between the types of abnormal TDP-43 immunoreactivities and the clinical course of the disease (age at onset and durations of illness). The GA of the neurons in the anterior horn cells of the spinal cord was adequately and specifically immunostained with the anti-TGN-46 antiserum. In controls, the GA of the anterior horn cells showed larger or angular profiles that filled the cell bodies (Fig. 1a2). All of the 48 neurons showing normal TDP-43 nuclear immunoreactivities (Type A) in ALS cases revealed normal GA profiles by TGN-46 immunostaining (Fig. 1b2). All of the 8 neurons with the loss of normal nuclear stainings and a few granular cytoplasmic TDP-43 immunoreactivities (Type B), and almost all of the 35 neurons with granular immunoreactivities for TDP-43 and no inclusions (Type C) also showed GA fragmentation (Fig. 1c2 and arrow in d2). All of the 50 neurons with skein-like or round inclusions (Type D) also exhibited the fragmentation of the GA (Fig. 1d2, arrowhead).

4. Discussion

TDP-43 was first cloned as a human protein capable of binding to TAR DNA of the human immunodeficiency virus 1 (HIV-1) long terminal repeat region [18]. TDP-43 interacts

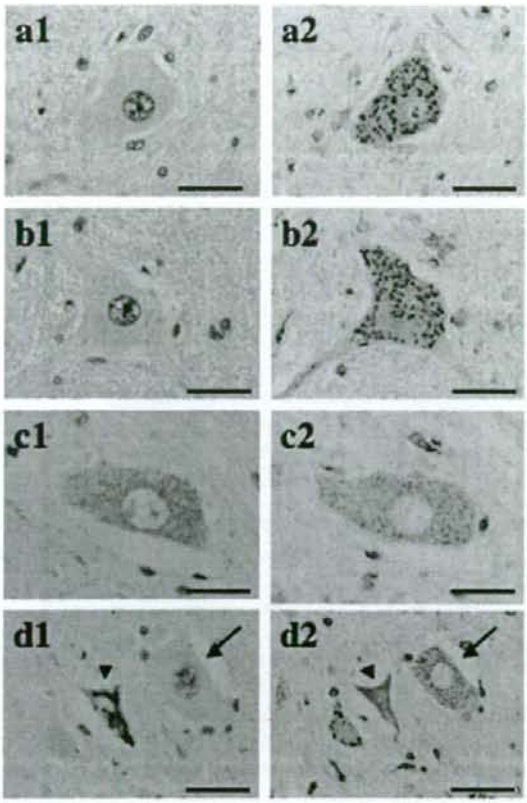

Fig. 1. Each mirror section of the spinal cord in control (a) and ALS cases (b–d). Immunostaining with anti-TDP-43 (a1–d1) and anti-TGN-46 antibodies (a2–d2). Neurons showing normal TDP-43 nuclear immunoreactivities (a1, b1) show normal GA profiles (a2, b2). A neuron showing the loss of normal nuclear staining and a few cytoplasmic TDP-43 immunoreactivities (d1, arrow), and a neuron with granular immunoreactivities for TDP-43 and no inclusions (c1) shows fragmentation of the GA (c2, arrow in d2). A neuron with a skein-like inclusion (d1, arrowhead) also showed the disappearance of the GA (d2, arrowhead). Bars: a–c 50 μm, d 30 μm.

with several nuclear ribonucleoproteins (RNP) including heterogeneous nuclear RNP A/B and survival motor neuron protein, inhibiting alternative splicing [19,20]. The physiological function of TDP-43 in the brain is currently unknown; however, recent studies have revealed that TDP-43 is a major component of neuronal cytoplasmic inclusions in motor neurons in ALS and FTLD-U [1,2]. Although the specific role of TDP-43 in neuronal degeneration remains obscure, a number of previous studies have suggested that this protein is directly involved in the pathogenesis of sporadic ALS, ALS with dementia, and FTLD-U [1,2,21,22]. In this study, we showed that the neurons with cytoplasmic TDP-43 immunostaining consistently demonstrated a loss of normal nuclear TDP-43 staining. Cytoplasmic localization of TDP-43 is pathologic since it is normally a DNA-binding protein located in the nucleus. We divided the anterior horn cells into four subtypes according to the differences of TDP-43 immunoreactivities: Type A: neurons showing normal nuclear staining, Type B: neurons exhibiting a loss of normal nuclear staining and a few granular cytoplasmic TDP-43 immunoreactivities, Type C: neurons showing a lot of granular TDP-43 immunoreactivities and no inclusions, and Type D: neurons with skein-like or round inclusions. Occasionally, anterior horn cells showed a loose aggregation of short threads of TDP-43-positive material, suggestive on an intermediate stage between the finely dispersed granular TDP-43 staining of cells without inclusions and the compacted rounded, spicular, or skein-like TDP-43 staining of the overt inclusions [21]. We speculate that the abnormal TDP-43 immunoreactivities lead to the loss of nuclear immunoreactivities at first, then aggregation in the shape of granules, and finally the formation of inclusion bodies.

On the other hand, the GA plays a key role in the transport, processing, and targeting of numerous proteins destined for secretion, the plasma membrane, and lysosomes [23,24]. In neurons, the GA is involved in the axoplasmic flow of numerous endogenous proteins and of exogenous macromolecules transported by orthograde, retrograde, and transsynaptic routes [25–27]. Therefore, GA fragmentation or loss will certainly have detrimental consequences on the functions of axons and presynaptic terminals. The fragmentation of the GA in human disease was first reported in sporadic ALS [5–7]. At present, GA fragmentation is not considered specific for ALS, since a similar lesion of the organelle was reported in Alzheimer's disease, corticobasal degeneration, and Parkinson's disease [17,28,29]. However, the neuronal GA is not dispersed in Alzheimer's disease in neurons with neurofibrillary tangles, and only 5% of the remaining substantia nigral neurons with Lewy bodies had the fragmented GA [28,29]. These findings are in contrast to a majority of motor neurons containing intracytoplasmic inclusions such as Bunina bodies, basophilic inclusions, and SOD1-positive aggregates which had fragmented GA [10,11,14]]. Therefore, we speculated that there was a correlation between intracytoplasmic inclusions and GA fragmentation in motor neuron disease. We herein demonstrated that all neurons showing normal TDP-43 nuclear immunoreactivities revealed normal GA profiles, and the majority of neurons with abnormal TDP-43 immunoreactivities showed GA fragmentation by TGN-46 immunostaining. Therefore, we considered that abnormal TDP-43 immunoreactivities are also correlated with GA fragmentation. However, recent studies have demonstrated the absence of cytoplasmic TDP-43 immunoreactivity in SOD1-related familial ALS cases. Lewy body-like hyaline inclusions observed in familial ALS were ubiquitinated, but negative for TDP-43 [30,31]. We previously reported that the GA of the anterior horn cells was fragmented in SOD1-related ALS patients [12]. Accordingly, we thought that GA fragmentation is a common mechanism of neuronal degeneration and has a strong relationship with abnormal TDP-43 immunoreactivities in ALS; however, abnormal TDP-43 was not directly involved in the maintenance of the GA structure.

We also demonstrated herein that almost all of the neurons showing a loss of normal nuclear staining, a few granular cytoplasmic immunoreactivities (Type B), and a lot of granular immunoreactivities and no inclusions (Type C) showed GA fragmentation. Neurons in Type B or C might be at an intermediate stage between neurons with normal nuclear staining for TDP-43 (Type A) and neurons with TDP-43-positive skein-like and round inclusions (Type D). These results provide supporting evidence that GA fragmentation occurs in the early stage of neuronal degeneration in ALS. Previous reports have indicated that GA fragmentation is associated with dysfunction of the secretory pathway, and that neuronal Golgi fragmentation is an early and probably irreversible lesion in neurodegeneration [15,32]. Thus, our results suggest that neurons without nuclear TDP-43 immunoreactivities are associated with dysfunction of the secretory pathway, and it is probably irreversible in the course of neuronal degeneration.

In the future, further morphological examinations of GA using electron microscopy are needed, and we have to clarify the significance of GA fragmentation in neurodegenerative disease.

Acknowledgement

This work was supported by grants from the Ministry of Health, Labour and Welfare of Japan, and also from the Ministry of Education, Culture, Sports, Science and Technology of Japan to K. Okamoto.

References

[1] Arai A, Hasegawa M, Akiyama H, Ikeda K, Nonaka T, Mori H, et al. TDP-43 is a component of ubiquitin-positive inclusions in frontotemporal lobar degeneration and amyotrophic lateral sclerosis. Biochem Biophys Res Commun 2006;351:602–11.

[2] Neumann M, Sampathu DM, Kwong LK, Truax AC, Micsenyi MC, Chou TT, et al. Ubiquitinated TDP-43 in frontotemporal lobar degeneration and amyotrophic lateral sclerosis. Science 2006;314:130–3.

[3] Croul S, Mezitis SGE, Stieber A, Chen YJ, Gonatas JO, Goud B, et al. Immunocytochemical visualization of the Golgi apparatus in several species, including human, and tissues with an antiserum against MG-160, a sialoglycoprotein of rat Golgi apparatus. J Histochem Cytochem 1990;38:957–63.

[4] Gonatas JO, Mezitis SGE, Stieber A, Fleischer B, Gonatas NK. MG-160: a novel sialoglycoprotein of the medial cisternae of the Golgi apparatus. J Biol Chem 1989;264:646–53.

[5] Gonatas NK, Stieber A, Mourelatos Z, Chen Y, Gonatas JO, Appel SH, et al. Fragmentation of the Golgi apparatus of motor neurons in amyotrophic lateral sclerosis. Am J Pathol 1992;140:731–7.

[6] Gonatas NK. Contributions to the Physiology of the Golgi apparatus. Am J Pathol 1994;145:751–61.

[7] Mourelatos Z, Adler H, Hirano A, Donnenfeld H, Gonatas JO, Gonatas NK. Fragmentation of the Golgi apparatus of motor neurons in amyotrophic lateral sclerosis revealed by organelle-specific antibodies. Proc Natl Acad Sci USA 1990;87:4393–5.

[8] Mourelatos Z, Yachnis A, Rorke L, Mikol J, Gonatas NK. The Golgi apparatus of motor neurons in amyotrophic lateral sclerosis. Ann Neurol 1993;33:608–15.

[9] Mourelatos Z, Hirano A, Rosenquist AC, Gonatas NK. Fragmentation of the Golgi apparatus of motor neurons in Amyotrophic Lateral Sclerosis (ALS). Clinical studies in ALS of Guam and experimental studies in deafferented neurons and in β, β′ iminidipropionitrile axonopathy. Am J Pathol 1994;144:1288–300.

[10] Stieber A, Chen Y, Weil S, Mourelatos Z, Gonatas JO, Okamoto K, et al. The fragmented neuronal Golgi apparatus in amyotrphic lateral sclerosis includes the trans-Golgi-network: functional implications. Acta Neuropathol 1998;95:245–53.

[11] Fujita Y, Okamoto K, Sakurai A, Kusaka H, Aizawa H, Mihara B, et al. The Golgi apparatus is fragmented in spinal cord motor neurons of amyotrophic lateral sclerosis with basophilic inclusions. Acta Neuropathol 2002;103:243–7.

[12] Fujita Y, Okamoto K, Sakurai A, Gonatas NK, Hirano A. Fragmentation of the Golgi apparatus of the anterior horn cells in patients with familial amyotrophic lateral sclerosis with SOD1 mutations and posterior column involvement. J Neurol Sci 2000;174:137–40.

[13] Mourelatos Z, Gonatas NK, Stieber A, Gurney ME, Dal Canto MC. The Golgi apparatus of spinal cord motor neurons in transgenic mice expressing mutant Cu, Zn superoxide dismutase (SOD) becomes fragmented in early, preclinical stages of the disease. Proc Natl Acad Sci USA 1996;93:5472–7.

[14] Fujita Y, Okamoto K. Golgi apparatus of the motor neurons in patients with ALS and in mice models of ALS. Neuropathol 2005;25:388–94.

[15] Gonatas NK, Stieber A, Gonatas JO. Fragmentation of the Golgi apparatus in neurodegenerative disease and cell death. J Neurol Sci 2006;246:21–30.

[16] Ponnambalam S, Girotti M, Yaspo M-L, Owen CE, Perry AC, Suganuma T, et al. Primate homologues of rat TGN38: primary structure, expression and functional implications. J Cell Sci 1996;109:675–85.

[17] Sakurai A, Okamoto K, Fujita Y, Nakazato Y, Wakabayashi K, Takahashi H, et al. Fragmentation of the Golgi apparatus of ballooned neurons in patients with corticobasal degeneration and Creutzfeldt–Jakob disease. Acta Neuropathol 2000;100:270–4.

[18] Ou SH, Wu F, Harrich D, Garcia-Martinez LF, Gaynor RB. Cloning and characterization of a novel cellular protein, TDP-43, that binds to human immunodeficiency virus type 1 TAR DNA sequence motifs. J Viol 1995;69:3584–96.

[19] Buratti E, Brindisi A, Giombi M, Tisminetzky S, Ayala YM, Baralle FE. TDP-43 binds heterogenous nuclear ribonucleoprotein A/B through its C-terminal tail. J Biol Chem 2005;280:37572–84.

[20] Wang IF, Rsddy NM, J Shen CK. Higher order arrangement of the eukaryotic nuclear bodies. Proc Natl Acad Sci USA 2002;99:13583–8.

[21] Davidson Y, Kelly T, Mackenzie IRA, Pickering-Brown S, Plessis DD, Neary D, et al. Ubiquitinated pathological lesions in frontotemporal lobar degeneration contain the TAR DNA-binding protein, TDP-43. Acta Neuropathol 2007;113:521–33.

[22] Neumann M, Kwong LK, Traux AC. TDP-43-positive white matter pathology in frontotenmporal lobar degeneration with ubiquitin-positive inclusions. J Neuropahol Exp Neurol 2007;66:177–83.

[23] Farquhar MG. Progress in unraveling pathways of Golgi traffic. Annu Rev Cell Biol 1985;1:447–88.

[24] Mellman I, Simons K. The Golgi complex: in vitro veritas? Cell 1992;68:829–40.

[25] Hammerschlag R, Stone GC, Bolen FA, Lindsay JD, Ellisman MH. Evidence that all newly synthesized proteins destined for fast axonal transport pass through the Golgi apparatus. J Cell Biol 1982;93:568–75.

[26] Rhodes CH, Stieber A, Gonatas NK. A quantitative electron microscopic study of the intracellular localization of wheat germ agglutinin in retinal neurons. J Comp Neurol 1986;254:287–96.

[27] Rhodes CH, Stieber A, Gonatas NK. Transneuronally transported wheat germ agglutinin labels glia as well as neurons in the rat visual system. J Comp Neurol 1987;261:460–5.

[28] Stieber A, Mourelatos Z, Gonatas NK. In Alzheimer's disease the Golgi apparatus of a population of neurons without neurofibrillary tangles is fragmented and atrophic. Am J Pathol 1996;148:415–26.

[29] Fujita Y, Ohama E, Takatama M, Al-Sarraj S, Okamoto K. Golgi apparatus of nigral neurons with α-synuclein-positive inclusions in patients with Parkinson's disease. Acta neuropathol 2006;112:261–5.

[30] Tan CF, Eguchi H, Tagawa A, Onodera O, Iwasaki T, Tsujino A, et al. TDP-43 immunoreactivity in neuronal inclusions in familial amyotrophic lateral sclerosis with or without SOD1 gene mutation. Acta Neuropathol 2007;113:535–42.

[31] Mackenzie IR, Bingo EH, Ince PG, Geser F, Neumann M, Cairns NJ, et al. Pathological TDP-43 distinguishes sporadic amyotrophic lateral sclerosis from amyotrophic lateral sclerosis with SOD1 mutations. Ann Neurol 2007;61:427–34.

[32] Stieber A, Gonatas JO, Moore JS, Bantly A, Yim HS, Yim MB, et al. Disruption of the structure of the Golgi apparatus and the function of the secretory pathway by mutants G93A and G85R of Cu, Zn superoxide dismutase (SOD1) of familial amyotrophic lateral sclerosis. J Neurol Sci 2004;219:45–53.

Cytokine 44 (2008) 293–297

Contents lists available at ScienceDirect

Cytokine

journal homepage: www.elsevier.com/locate/issn/10434666

Time lag between the increase of IL-6 with fever and NF-κB activation in the peripheral blood in inflammatory myofibroblastic tumor

Reiji Fukano [a], Tomoyo Matsubara [a,*], Takashi Inoue [b], Toshikazu Gondo [c], Takashi Ichiyama [a], Susumu Furukawa [a]

[a] Department of Pediatrics, Yamaguchi University Graduate School of Medicine, 1-1-1 Minamikogushi, Ube, Yamaguchi 755-8505, Japan
[b] First Department of Surgery, Yamaguchi University Graduate School of Medicine, Japan
[c] First Department of Pathology, Yamaguchi University Graduate School of Medicine, Japan

ARTICLE INFO

Article history:
Received 7 February 2008
Received in revised form 14 August 2008
Accepted 29 August 2008

Keywords:
IL-6
Inflammatory myofibroblastic tumor (IMT)
Intermittent fever
Peripheral blood mononuclear cells
NF-κB activation

ABSTRACT

We describe a case of inflammatory myofibroblastic tumor (IMT) that occurred in the retroperitoneum. The patient manifested systemic symptoms, such as intermittent fever, anemia, thrombocytosis, and hypergammaglobulinemia. In order to elucidate the mechanism of intermittent fever in IMT, we analyzed nuclear factor-kappa B (NF-κB) activation in peripheral blood mononuclear cells (PBMCs) using flow cytometry, and serum cytokine levels. NF-κB activation was observed in the peripheral blood T cells and monocytes/macrophages. Among the measured cytokines, only interleukin (IL)-6 levels were elevated. IL-6 levels during pyrexia in the afternoon were higher than those during apyrexia in the morning. In contrast to IL-6, NF-κB activation in PBMCs was lower during pyrexia than during apyrexia; this is considered to be because the activation is subject to negative feedback. The time lag between the increase of IL-6 in the serum and NF-κB activation in the PBMCs at the onset of intermittent fever in IMT may provide further insight into the role of cytokines and NF-κB activation in febrile inflammatory diseases.

1. Introduction

Inflammatory myofibroblastic tumor (IMT), previously described as an inflammatory pseudotumor, has been defined in the recent World Health Organization classification of soft tissue tumors [1]. This tumor is a distinctive lesion comprised of differentiated myofibroblastic spindle cells, usually accompanied by the inflammatory infiltration of plasma cells, lymphocytes, and eosinophils, which occurs primarily in the soft tissue and viscera of young adults and children [2–5]. The symptoms and manifestations are related to the tumor location [6]. Of the cases reported in the literature, 19% were accompanied by some type of systemic symptom, including fever, anemia, thrombocytosis, weight loss, hypergammaglobulinemia, and increased erythrocyte sedimentation rate [7,8]. Previous studies have demonstrated overproduction of interleukin (IL)-6 and IL-1 in the tumor [9–11].

It is well known that fever is modified by the release of large amounts of proinflammatory cytokines, such as tumor necrosis factor-α (TNF-α), IL-1, and IL-6, into the blood. Nuclear factor-kappa B (NF-κB) is a ubiquitous transcription factor for genes that encode proinflammatory cytokines [12–14]. The prototype of NF-κB is a heterodimer consisting of p50 and p65 bound by members of the IκB family, including IκBα, in the cytoplasm [15,16]. Phosphorylation of IκB by bacterial products, viruses, drugs, or cytokines rapidly leads to its degradation and translocation of NF-κB to the nucleus [17,18]. Activation of NF-κB results in the binding of specific promoter elements and the expression of mRNAs for proinflammatory cytokine genes [17,18].

In this study, we describe a case of abdominal IMT in a female child in whom intermittent fever was persisted. In order to elucidate the mechanism of intermittent fever in IMT, we analyzed NF-κB activation in the peripheral blood, and the serum levels of cytokines in a patient with IMT.

1.1. Case reports

A previously healthy 5-year-old girl was referred to the Yamaguchi University Graduate School of Medicine with the chief complaint of intermittent fever that had persisted for 2 weeks. Daily, her body temperature rose to 39 °C in the afternoon and dropped to below 37 °C in the morning (Fig. 1). Physical examination on admission revealed no abnormalities. The white blood cell (WBC) count was 11,430/mm^3, with differential leukocyte counts of 2% band neutrophils, 68% segmented neutrophils, and 22.5% lymphocytes. The level of hemoglobin was 8.5 g/dl; hematocrit, 28.1%; and serum iron; 12 μg/dl. The platelet count was 665,000/mm^3, and the level of C-reactive protein was 11.31 mg/dl. Serum

* Corresponding author. Fax: +81 836 22 2257.
E-mail address: tmatsu@yamaguchi-u.ac.jp (T. Matsubara).

1043-4666/$ - see front matter © 2008 Elsevier Ltd. All rights reserved.
doi:10.1016/j.cyto.2008.08.016

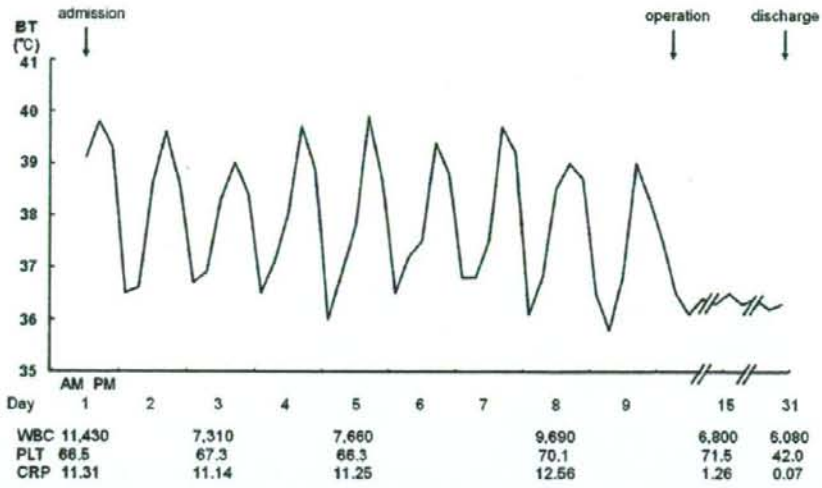

Fig. 1. Clinical course of the patient. Daily, the patient's body temperature (BT) rose to 39 °C in the afternoon and dropped to below 37 °C in the morning. Her BT dropped rapidly after the operation. Laboratory data improved immediately after the operation. BT, body temperature; WBC, white blood cell count (/mm^3); PLT, platelet count (10^4/mm^3); CRP, C-reactive protein (mg/dl).

levels of IgG and IgA were found to be elevated to as high as 1485 and 536 mg/dl, respectively; however, IgM and IgE levels were within the normal ranges. Tests for the presence of human herpes virus 8 (HHV8) and Epstein–Barr virus (EBV) DNA in peripheral blood—as determined by the polymerase chain reaction—were both negative. The patient underwent bone marrow aspiration; the results revealed a normocellular marrow with no evidence of dysplasia.

Ultrasonographic examination of the abdomen revealed a localized mass in the anteromedial aspect of the left kidney. Computed tomography of the abdomen revealed a 4 × 4 cm round mass located in the left adrenal gland (Fig. 2). An unenhanced scan revealed that the mass was homogeneous and isoattenuated relative to the kidney. There was no evidence of calcification in the mass. T1- and T2-weighted MRI images revealed that the mass was isointense relative to the spleen. On the 9th day of admission, the patient underwent surgery. The tumor, which had originated in the retroperitoneum, was situated posterior to the pancreas, and was firmly adherent to the left adrenal gland. Complete resection of the mass together with the left adrenal gland was performed.

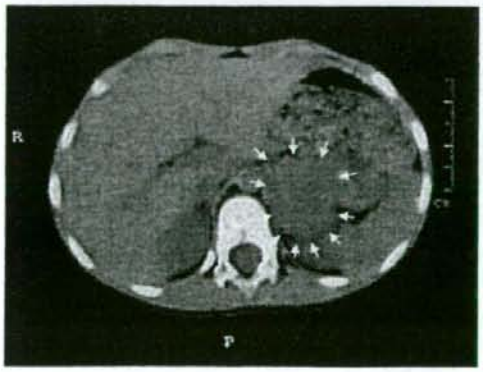

Fig. 2. Computed tomography and the resected tumor. Computed tomography of the abdomen revealed a 4 × 4 cm round mass in the left adrenal gland. The mass was homogeneous and isoattenuated relative to the kidney.

On staining with hematoxylin and eosin, spindled myofibroblasts and plasma cells were observed in an edematous myxoid background characterized by abundant vasculature (Fig. 3a). Some areas were characterized by compact fascicular spindle cell proliferation with variable myxoid and collagenized regions, and regions infiltrated with eosinophils, plasma cells, and lymphocytes. Immunohistochemical cytoplasmic positivity for anaplastic lymphoma kinase (ALK) was detected in approximately 50% of the myofibroblasts using monoclonal ALK1 antibodies (Dako, Kyoto, Japan) (Fig. 3b). Fifty percent of the plasma cells exhibited diffuse cytoplasmic reactivity for IgG and IgA. In addition, the tumor specimen was examined using transmission electron microscopy. The tumor cells exhibited the ultrastructural features of myofibroblastic and fibroblastic differentiation (Fig. 3c). The pathological diagnosis was IMT.

Post-operatively, the patient's body temperature dropped rapidly to 36 °C and did not rise again. The platelet count and the level of C-reactive protein (CRP) returned to normal (Fig. 1). Subsequently, the patient was discharged on the 21st post-operative day.

2. Materials and methods

2.1. Materials

Informed consent was obtained from the patient's parents. Peripheral blood samples were taken during apyrexia in the morning and during pyrexia in the afternoon.

2.2. Methods

2.2.1. NF-κB activation in PBMCs

As reported previously, the expression of NF-κB in PBMCs was measured by flow cytometry [19–21]. Peripheral blood cells were labeled with a phycoerythrin (PE)-conjugated anti-CD14 monoclonal antibody, a peridinin chlorophyll protein (PerCP)-conjugated anti-CD3 monoclonal antibody, a PE-conjugated anti-CD4 monoclonal antibody, or a PerCP-conjugated anti-CD8 monoclonal antibody, and then permeabilized with 4% paraformaldehyde in phosphate-buffered saline, pH 7.2, containing 0.1% saponin and 10 mM Hepes. The cells were labeled with mouse anti-NF-κB (nu-

Fig. 3. Histopathology of the tumor. (a) Hematoxylin and eosin staining under high-power magnification (original magnification 400×). The tumor comprised myofibroblastic spindle cells proliferating in an inflammatory stroma of lymphocytes and plasma cells. (b) Immunostaining for anaplastic lymphoma kinase (ALK). ALK was positive in the cytoplasm of myofibroblastic spindle cells. (c) Electron microscopy. The tumor cell displayed ultrastructural features of myofibroblastic differentiation (c).

clear-localized signal) antibody (IgG3; CHEMICON, Temecula, CA). The mouse anti-NF-κB (nuclear-localized signal) antibody recognizes an epitope overlapping the nuclear location signal of NF-κB-p65 and therefore selectively recognizes the activated form of NF-κB. The cells were then labeled with a fluorescein isothiocyanate-conjugated rat anti-mouse IgG3 monoclonal antibody (BD PharMingen, San Diego, CA). After being washed, the cells were fixed with 1% paraformaldehyde in PBS and stored at 4 °C until the flow cytometric analysis. Immunofluorescence staining was analyzed with a FACScan flow cytometer equipped with CellQuest software. We analyzed 5000 cells for each sample by flow cytometry.

2.3. Serum levels of cytokines

The serum level of IL-1β was determined by enzyme-linked immunosorbent assay using commercially available kits (R&D Systems Co, Minneapolis, USA and Bender Med Systems, Vienna, Austria). The concentrations of IL-2, IL-4, IL-6, IL-10, IL-12, interferon-gamma (IFN-γ), and TNF-α were measured by flow cytometry using a cytometric bead array kit (BD PharMingen, San Diego, CA).

2.4. Statistical analysis

The data were statistically analyzed using the Mann–Whitney *U* test and Student's *t*-test for comparison of the means.

3. Results

3.1. The percentage of cells exhibiting NF-κB activity

Fig. 4 shows all flow cytometric analyses of $CD4^+$ T cells, $CD8^+$ T cells, and $CD14^+$ monocytes/macrophages exhibiting NF-κB activity. The percentage of $CD4^+$T cells, $CD8^+$T cells, and $CD14^+$ monocytes/macrophages exhibiting NF-κB activity during apyrexia was 70.1 ± 1.3% (mean ± SD), 84.0 ± 5.1%, and 58.8 ± 5.2%, respectively (Table 1). The percentage of $CD4^+$, $CD8^+$, and $CD14^+$ cells exhibiting NF-κB activity in the patient during pyrexia was 24.4 ± 5.3%, 40.0 ± 5.4%, and 22.1 ± 2.0%, respectively. These percentages were extremely high in comparison with the normal ranges, being 0.7–6.3%, 0.2–4.2%, and 0.6–5%, as previously reported [21]. The percentage of $CD4^+$, $CD8^+$, and $CD14^+$ cells exhibiting NF-κB activity increased to a greater degree during apyrexia than during pyrexia ($p < 0.05$).

3.2. Serum levels of cytokines

The serum levels of IL-6 increased as high as 238.7 ± 34.5 pg/ml (mean ± SD) during pyrexia and 102.1 ± 53.7 pg/ml during apyrexia (normal range; <19.9 pg/ml) (Table 1). The IL-6 levels were significantly higher during pyrexia than during apyrexia ($p < 0.05$). There was no increase in the serum levels of IL-1β (normal range, <3.9 pg/ml), IL-2 (<4.5 pg/ml), IL-4 (<15.0 pg/ml), IL-8 (<3.6 pg/ml), IL-10 (<14.2 pg/ml), IL-12 (<26.5 pg/ml), IFN-γ (<42.9 pg/ml), or TNF-α (<11.1 pg/ml). On the 6th post-operative day, the serum level of IL-6 decreased rapidly to a minimum of 15.5 pg/ml.

4. Discussion

In this study, we report a case of IMT that occurred in the retroperitoneum. The characteristics of the histopathological findings in our case were typical of IMT [1–4]. The etiology of IMT remains unclear, with some investigators considering it as an immunological response to infectious agents including HHV8 and EBV [5,11]. However, neither HHV8 nor EBV was detected in our patient.

The patient manifested systemic symptoms, such as intermittent fever, anemia, thrombocytosis, and hypergammaglobulinemia. Regarding these symptoms, we focused on intermittent fever in this study. Only serum IL-6 levels were increased among the cytokines that were examined, which included IL-1β, IL-2, IL-4, IL-6, IL-10, IL-12, IFN-γ, and TNFα. The elevation of serum IL-1β and/or IL-6 levels has previously reported in some cases of IMT [9,11]. Overexpression of IL-6 in IMT tissue was also reported [9,10]. We suspect that the tumor in our case produced IL-6, while we did not examine IL-6 expression in the tumor. The serum IL-6 levels during pyrexia in the afternoon were higher than those during apyrexia in the morning. In inflammatory or infectious diseases in general, many proinflammatory cytokines, such as IL-1β, IL-6, and TNF-α, are elevated in the sera and mediate the febrile response. Since only IL-6 was increased in our patient with IMT, the changes in the serum IL-6 levels were directly related to the febrile response.

There was massive NF-κB activation in the PBMCs. Regarding NF-κB activation in PBMCs, we have reported that NF-κB activation in PBMCs measured by flow cytometry is similar to that detected by Western blot analysis [21]. In addition, there are some representative reports on NF-κB activation in peripheral blood by flow cytometry [19,22,23]. NF-κB activation in the peripheral blood $CD4^+$T cells, $CD8^+$T cells, and $CD14^+$monocytes/macrophages was increased during both apyrexia and pyrexia in the present study. In particular, NF-κB activation was remarkable in T cells during apyrexia. We have already reported that NF-κB activation in PBMCs increased in patients with inflammatory diseases, such as Kawasaki disease [21], chronic infantile neurological, cutaneous, articular syndrome [24] and sepsis [25]. The percentage of NF-κB activation in PBMCs in IMT was higher than in these inflammatory diseases. We speculate that IL-6 produced in IMT tissue may in-

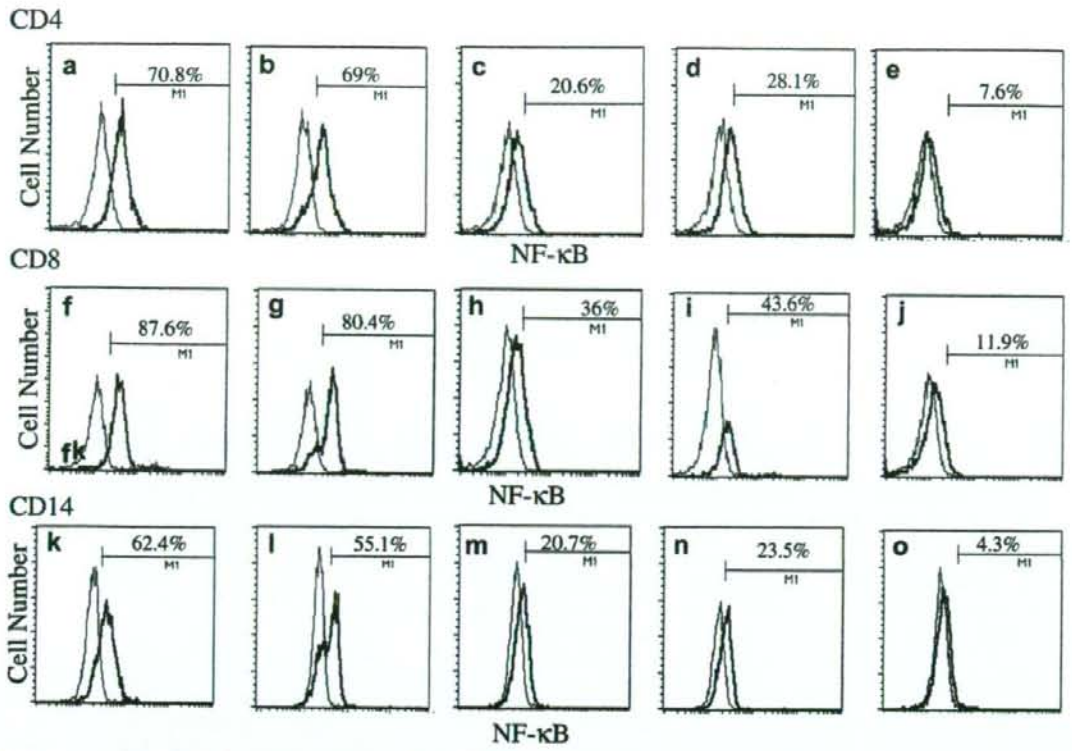

Fig. 4. The percentage of cells with NF-κB activation in peripheral blood $CD4^+$ T cells, $CD8^+$ T cells, and $CD14^+$ monocytes/macrophages as determined by flow cytometri analysis. (a and b) $CD4^+$ T cells during apyrexia before the surgery. (c and d) $CD4^+$ T cells during pyrexia before the surgery. (e) $CD4^+$ T cells after the surgery. (f and g) $CD8^+$ cells during apyrexia before the surgery. (h and i) $CD8^+$ T cells during pyrexia before the surgery. (j) $CD8^+$ T cells after the surgery. (k and l) $CD14^+$ monocytes/macrophage during apyrexia before the surgery. (m and n) $CD14^+$ monocytes/macrophages during pyrexia before the surgery. (o) $CD14^+$ monocytes/macrophages after the surgery.

Table 1
Serum levels of IL-6 and NF-κB activation in peripheral blood mononuclear cells

	Pre-surgery		Post-surgery
	Apyrexia	Pyrexia	
Serum levels (pg/ml)	$n = 5$	$n = 4$	$n = 1$
IL-6 [<19.9]	102.1 ± 53.7	238.7 ± 34.5	2.8
NF-κB activation (%)*	$n = 2$	$n = 2$	$n = 1$
$CD4^+$ T cells [0.7–6.3]	70.0 ± 1.3	24.4 ± 5.3	7.6
$CD8^+$ T cells [0.2–4.2]	84.0 ± 5.1	40.0 ± 5.4	11.9
$CD14^+$ monocytes [0.6–5.0]	58.8 ± 5.2	22.1 ± 2.0	4.3

Results of pre-surgery represent the averages and standard deviations.
Values in brackets represent normal ranges.
IL, interleukin; NF-κB, nuclear factor-kappa B.
* The percentage of cells with NF-κB activation in $CD4^+$, $CD8^+$, and $CD14^+$ cells.

duce NF-κB activation in PBMCs to produce more IL-6 in circulation, and continuously increase the massive NF-κB activation in PBMCs.

We investigated the change of NF-κB activation in the PBMCs and serum IL-6 levels in relation to the intermittent fever. The serum IL-6 levels during pyrexia were higher than those during apyrexia. In contrast, NF-κB activation in the PBMCs was lower during pyrexia than during apyrexia. We speculate that the reason for this negative correlation between serum IL-6 levels and NF-κB activation in the PBMCs is as follows: IL-6 overproduction followed by NF-κB activation in the PBMCs during apyrexia in the morning caused pyrexia in the afternoon. NF-κB up-regulates the transcription of its inhibitor, namely IκB [17]. As a result, the suppression o NF-κB activation by IκB might occur during pyrexia in the afternoon. Further study concerning IκB is needed to support thi hypothesis.

In conclusion, we analyzed the NF-κB activation in PBMCs anc serum cytokine levels in a patient with abdominal IMT. In particular, we demonstrated that the time lag between the increase of IL-6 in the serum and NF-κB activation in the PBMCs was observed a the onset of intermittent fever in IMT. This in vivo study provec useful in obtaining further insight into the role of cytokines anc NF-κB activation in febrile inflammatory diseases.

Acknowledgments

The authors thank Yoshiko Ueno (Department of Pediatrics Yamaguchi University Graduate School of Medicine) for her valuable assistance with the experiments.

References

[1] Coffin CM, Flether JA. Inflammatory myofibroblastic tumor. In: Fletcher CDM Unni KK, Mertens F, editors. World Health Organization classification o tumors: pathology and genetics of tumor of soft tissue and bone. Lyon France: IARC press; 2002. p. 91–3.
[2] Karnak I, Senocak ME, Ciftci AO, Caglar M, Bingöl-Kologlu M, Tanyel FC, et al. Inflammatory myofibroblastic tumor in children: diagnosis and treatment. J Pediatr Surg 2001;36:908–12.
[3] Janik JS, Janik JP, Lovell MA, Hendrickson RJ, Bensard DD, Greffe BS. Recurrent inflammatory pseudotumors in children. J Pediatr Surg 2003;38:1491–5.

[4] Morotti RA, Legman MD, Kerkar N, Pawel BR, Sanger WG, Coffin CM. Pediatric inflammatory myofibroblastic tumor with late metastasis to the lung: case report and review of the literature. Pediatr Dev Pathol 2005;8:224–9.
[5] Mergan F, Jaubert F, Sauvat F, Hartmann O, Lortat-Jacob S, Révillon Y, et al. Inflammatory myofibroblastic tumor in children: clinical review with anaplastic lymphoma kinase, Epstein-Barr virus, and human herpesvirus 8 detection analysis. J Pediatr Surg 2005;40:1581–6.
[6] Narla LD, Newman B, Spottswood SS, Narla S, Kolli R. Inflammatory psuedtumor. RadioGraphics 2003;23:719–29.
[7] Kutluk T, Emir S, Karnak I, Gağlar M, Büyükpamukçu M. Mesentric inflammatory psuedotumor: usual presentation with leukemoid reaction and massive calcified mass. J Pediatr Hematol Oncol 2002;24:158–9.
[8] Chun YS, Wang L, Nascimento AG, Moir CR, Rodeberg DA. Pediatric inflammatory myofibroblastic tumor: anaplastic lymphoma kinase (ALK) expression and prognosis. Pediatr Blood Cancer 2005;45:796–801.
[9] Rohrlich P, Peuchmaur M, de Napoli-Cocci S, Gasselin ID, Garel C, Aigrain Y, et al. Interleukin-6 and interleukin-1β production in a pediatric plasma cell granuloma of lung. Am J Surg Pathol 1995;19:590–5.
[10] Azuno Y, Yaga K, Suehiro Y, Ariyama S, Oga A. Inflammatory myofibroblastic tumor of the uterus and interleukin-6. Am J Obstet Gynecol 2003;189:890–1.
[11] Gomez-Roman JJ, Sanchez-Velasco P, Ocejo-Vinyals G, Hernández-Nieto E, Leyva-Cobián F, Val-Bernal JF. Human herpesvirus-8 genes are expressed in pulmonary inflammatory myofibroblastic tumor (inflammatory pseudotumor). Am J Surg Pathol 2001;25:624–9.
[12] Collart MA, Baeuerle P, Vassali P. Regulation of tumor necrosis factor alpha transcription in macrophages: involvement of four κB-like motifs and of constitutive and inducible forms of NF-κB. Mol Cell Biol 1990;10:1498–506.
[13] Libermann TA, Baltimore D. Activation of interleukin-6 gene expression through the NF-κB transcription factor. Mol Cell Biol 1990;10:2327–34.
[14] Hiscott J, Marois J, Garoufalis J, D'Addario M, Roulston A, Kwan I, et al. Characterization of a functional NF-κB site in the human interleukin 1β promotor: evidence for a positive autoregulatory loop. Mol Cell Biol 1993;13:6231–40.
[15] Matsusaka T, Fujikawa K, Nishio Y, Mukaida N, Matsushima K, Kishimoto T, et al. Transcription factors NF-IL6 and NF-κB synergistically activate transcription of the inflammatory cytokines, interleukin 6 and interleukin 8. Proc Natl Acad Sci USA 1993;90:10193–7.
[16] Baeuerle PA, Henkel T. Function and activation of NF-κB in the immune system. Annu Rev Immunol 1994;12:141–79.
[17] Baldwin Jr AS. The NF-κB and IκB proteins: new discoveries and insights. Annu Rev Immunol 1996;14:649–83.
[18] Brown K, Gerstberger S, Carlson L, Franzoso LG, Siebenlist U. Control of IκB-α proteolysis by site-specific, signal-induced phosphorylation. Science 1995;267:1485–8.
[19] Foulds S. Novel flow cytometric method for quantifying nuclear binding of the transcription factor nuclear factor kappa B in unseparated human monocytes and polymorphonuclear cells. Cytometry 1997;29:182–6.
[20] Pyatt DW, Stillman WS, Yang Y, Gross S, Zheng JH, Irons RD. An essential role for NF-kappaB in human CD34(+) bone marrow cell survival. Blood 1999;93:3302–8.
[21] Ichiyama T, Yoshitomi T, Nishikawa M, Fujiwara M, Matsubara T, Hayashi T, et al. NF-κB activation in peripheral blood monocytes/macrophages and T cells during acute Kawasaki disease. Clin Immunol 2001;99:373–7.
[22] Lafarge S, Hamzeh-Cognasse H, Chavarin P, Genin C, Garraud O, Cognasse F. A flow cytometry technique to study intracellular signals NF-kappaB and STAT3 in peripheral blood mononuclear cells. BMC Mol Biol 2007;8:64.
[23] García-García E, Rosales C. Nuclear factor activation by FcgammaR in human peripheral blood neutrophils detected by a novel flow cytometry-based method. J Immunol Methods 2007;320:104–18.
[24] Matsubara T, Hasegawa M, Shiraishi M, Hoffman HM, Ichiyama T, Tanaka T, et al. A severe case of chronic infantile neurologic, cutaneous, articular syndrome treated with biologic agents. Arthritis Rheum 2006;54:2314–20.
[25] Hotta N, Ichiyama T, Shiraishi M, Takekawa T, Matsubara T, Furukawa S. Nuclear factor-kappaB activation in peripheral blood mononuclear cells in children with sepsis. Crit Care Med 2007;35:2395–401.

Neuron-specific and inducible recombination by Cre recombinase in the mouse

Yukiko Hashimoto[a,b], Kazuhiro Muramatsu[a], Takefumi Uemura[a], Reiko Harada[a], Takashi Sato[a], Koichi Okamoto[b] and Akihiro Harada[a]

[a]Laboratory of Molecular Traffic, Department of Molecular and Cellular Biology, Institute for Molecular and Cellular Regulation, Gunma University and [b]Department of Neurology, Gunma University Graduate School of Medicine, Maebashi, Gunma, Japan

Correspondence to Akihiro Harada, Laboratory of Molecular Traffic, Department of Molecular and Cellular Biology, Institute for Molecular and Cellular Regulation, Gunma University, 3-39-15 Showa, Maebashi, Gunma 371-8512, Japan
Tel: +81 27 220 8840; fax: +81 27 220 8844; e-mail: aharada@showa.gunma-u.ac.jp

Received 10 January 2008; accepted 4 February 2008

To investigate the neuronal function of genes *in vivo*, a neuron-specific and inducible gene targeting system is desirable. In this study, we generated a knockin mouse line that expresses a fusion protein consisting of the Cre recombinase and the progesterone receptor (CrePR) in neurons. The neuron-specific expression of CrePR was attained by inserting *CrePR* gene into the τ locus, because τ is expressed strongly in neurons but scarcely in glias and other tissues. By crossing this knockin mouse line (τ^{CrePR}) with *ROSA26* lacZ reporter mouse line (*R26R*), we observed that the antiprogesterone RU486 could induce recombinase activity of the CrePR specifically in neurons. Thus, τ^{CrePR} knockin line is a useful tool for studying neuronal gene functions. *NeuroReport* 19:621–624 © 2008 Wolters Kluwer Health | Lippincott Williams & Wilkins.

Keywords: conditional knockout, Cre recombinase, gene targeting, knockin, neuron, progesterone receptor, RU486, τ

Introduction

Gene targeting is useful for analyzing the molecular functions of a gene *in vivo*. Knocking out the gene of interest in the entire body sometimes, however, leads to embryonic lethality, preventing further investigation. To circumvent this problem, conditional knockout technology is now widely used. To delete genes in a neuron-specific manner, various Cre transgenic mice have been generated such as nestin-Cre [1], neurofilament H-Cre [2], and synapsin1-Cre mice [3].

To acquire additional temporal control of gene targeting, the tamoxifen-inducible Cre recombinase ($CreER^T$) has been developed [4]. Recently, Kellendonk *et al.* [5,6] reported that the RU486-inducible Cre recombinase and the progesterone receptor (CrePR) had the same or even better regulatory properties than $CreER^T$. In this CrePR/loxP system, the *Cre* gene and the mutated ligand-binding domain of the human progesterone receptor gene were fused to produce the *CrePR* gene [7]. The recombinase activity of the CrePR is induced by the synthetic antiprogesterone RU486, but not by endogenous progesterone. This system would make it possible to delete the specific gene at any desirable time. It also permits studies in the same mouse before and after deletion of the gene.

Several CrePR mice have been reported so far, including Ca^{2+}/calmodulin-dependent kinase II-CrePR (induced in cortex and hippocampus neurons) [6], L-*N*-methyl-D-aspartate-type glutamate receptor GluR ε_3 subunit-CrePR (cerebellar granule cell-specific) [8], and GluR δ_2-CrePR (Purkinje cell specific) [9,10]. All these strains are useful for spatiotemporally controlled gene targeting in the nervous system, but in either of these lines, the recombination is limited to specific member of neurons. Therefore, a mouse line is required that can induce temporal control of recombination in all types of neurons.

In this study, we have established a knockin mouse line named τ^{CrePR}, which expresses CrePR specifically in neurons by inserting the *CrePR* gene in the τ locus. The τ locus is suitable for our purpose because τ, a microtubule-associated protein, is expressed strongly in neurons but scarcely in glial and other tissues. Moreover, our earlier study has demonstrated that τ knockout mice exhibited a very subtle phenotype in the nervous system [11]. Here, we show that the recombination of τ^{CrePR} line is neuron-specific and inducible, thus providing a useful tool for studying neuronal gene functions.

Materials and methods

Generation of τ-CrePR knockin mice

All animal procedure were performed in accordance with the guidelines of the Animal Care and Experimentation Committee of Gunma University, and all animals were bred in the Institute of Animal Experience Research of Gunma University. We used a 10-kb *Eco*RI fragment containing the τ gene obtained from the 129/Sv mouse genomic library and subcloned into pGEM7Zf(+) (Promega, Fitchburg, Wisconsin, USA) as the source of the genomic fragment of the τ gene [11]. The 673 bp 5′ untranslated region of the τ gene amplified by PCR was ligated in-frame into the 67 bp oligo fragment encoding the initial methionine, the nuclear localization signal (NLS) of SV40 large T antigen, and the

amino acid residues 2–13 of Cre recombinase. The 740 bp *SalI-AgeI* PCR-oligo fragment was ligated to the *AgeI-XhoI* fragment of the CrePR [8]. An 8.2 kb genomic fragment was ligated into the 3′ end of NLS-CrePR cDNA. Finally, phosphoglycerokinase-neo cassette (PGK-Neo-pA) flanked by flippase recognition target sites was ligated into the *XhoI* site adjacent to the NLS-CrePR cDNA to generate the knockin vector.

Embryonic stem (ES) cells were cultured on neomycin-resistant mouse embryonic fibroblasts in ES medium as described previously [11]. The targeting vector was linearized by *NotI* and electroporated into the ES cells using Gene Pulser (Bio-Rad, Hercules, California, USA). G418 selection (175 mg/ml) was started 38–48 h after the electroporation.

Genomic DNA from G418-resistant clones digested with *BamHI* was analyzed for homologous recombination by Southern blotting in accordance with standard protocols [11]. A 500-bp *EcoRI/SmaI* fragment whose 5′ end was located 2.8 kb upstream of exon I, indicated as 'probe' in Fig. 1b, was used for screening of genomic DNA. Furthermore, a 600-bp fragment in PGK-neo-pA was used as the internal probe to check the integrity of the targeted allele. The targeting strategy is shown in Fig. 1.

Genotyping of τ-CrePR knockin mice

PCR analysis was used for detection of the wild-type and targeted alleles. When we used Cre primers 1 (Cre F: AGGTTCGTTCTCTCATGGA) and 2 (Cre R: TCGAC CAGTTTAGTTACCC) for detection of the knockin allele, a 250 bp product was amplified. To confirm the presence of the wild-type allele, we used mτ primers 3 (mτ F: TATGGCTGACCCTCGCCAGGAGTTT) and 4 (mτ R: GTCCACCCCACTGACCTTTTAAGCC).

Analysis of CrePR-mediated recombination efficacy

We used the mutant mice containing τ-*CrePR* and *Rosa26* transgene heterozygously ($\tau^{CrePR}/+$; *R26R*/+). The antiprogesterone RU486 suspension was prepared as described previously [9]. We injected 1 mg/g body weight of RU486 into 6-week-old mutant mice intraperitoneally for two consecutive days. The mice were transcardially perfused with 3% paraformaldehyde, and the tissues were postfixed and cryoprotected as described previously [12]. The frozen sections (10 μm) were incubated with rabbit polyclonal anti-β-galactosidase (β-gal) antibody (Cappel, Durham, North Carolina, USA) and mouse monoclonal anti-neuronal nuclei antibody (Chemicon, Temecula, California, USA), followed by the incubation with Alexa 568-conjugated anti-rabbit IgG antibody (Invitrogen, San Diego, California, USA) and Alexa 488-conjugated anti-mouse IgG antibody (Invitrogen). The sections were observed using a laser scanning confocal microscope (model MRC-1024; Zeiss, Oberkochen, Germany), and the images were processed digitally using Adobe Photoshop (Adobe Systems, San Jose, California, USA).

For X-gal histochemistry, the sections were washed in X-gal rinse buffer [5 mM ethylene glycol-bis (pH 8.0), 2 mM $MgCl_2$, 0.02% NP40, and 0.01% deoxycholate in PBS], and were stained overnight at 37°C with X-gal staining buffer (5 mM potassium ferricyanide, 5 mM potassium ferrocyanide, and 1.0 mg/ml X-gal in X-gal rinse buffer).

Results

Generation of CrePR knockin mice

To generate a neuron-specific and inducible gene targeting system, we established a knockin mouse line named τ^{CrePR}, which carries the *CrePR* gene in the τ locus (Fig. 1a). The *CrePR* gene expresses the Cre recombinase fused to a truncated form of the human progesterone receptor ligand-binding domain. The activity of this recombinase is highly dependent on the presence of RU486, but not influenced by endogenous hormones [5,6].

We constructed a targeting vector in which *CrePR* gene was inserted in the translation initiation site of the τ gene in frame (Fig. 1b). The targeting vector was linearlized and electroporated into ES cells. The targeting efficiency was about 65%. Homologous recombinant ES cells (Fig. 1c) were cultured and injected into blastocysts as described previously [11]. Similar to τ knockout mice, the mutant mice homozygous for the knockin allele ($\tau^{CrePR/CrePR}$) were fertile and showed no evidence of premature mortality [11]. Their brain weight was similar to that of their littermate controls.

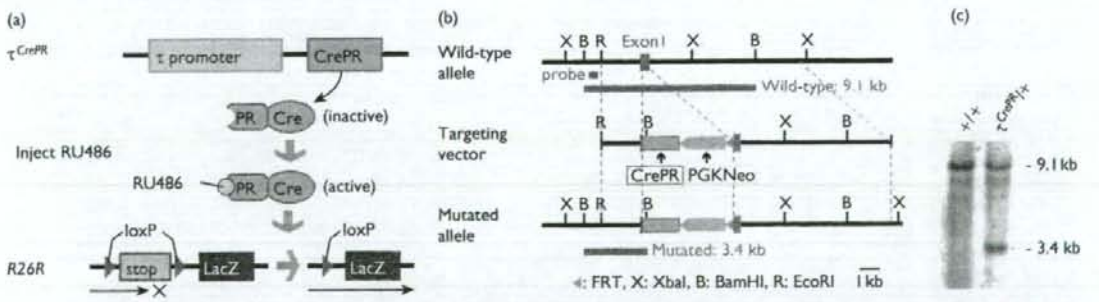

Fig. 1 Generation of τ^{CrePR} knockin mouse. (a) Scheme for the induction of Cre recombinase of τ^{CrePR} mouse by antiprogesterone RU486, and the mating scheme used to analyze the recombination activity by *R26R* mouse. (b) Schematic representation of mouse τ wild-type (WT) allele (top), knockin vector (middle), and targeted allele (bottom). Targeting strategy used for inserting *CrePR* gene in-frame immediately downstream of initiating ATG in exon I of the τ gene. The neomycin resistance cassette (neo) was flanked by two FRTs to enable the flippase-mediated excision of this selective marker. (c) Southern blotting of representative genomic DNA of ES cells. Genomic DNA was digested with *BamHI*, and Southern blot analysis was performed using 5′ flanking probe, which is indicated in (b). CrePR, Cre recombinase and the progesterone receptor; ES, embryonic stem; FRT, flippase recognition target site.

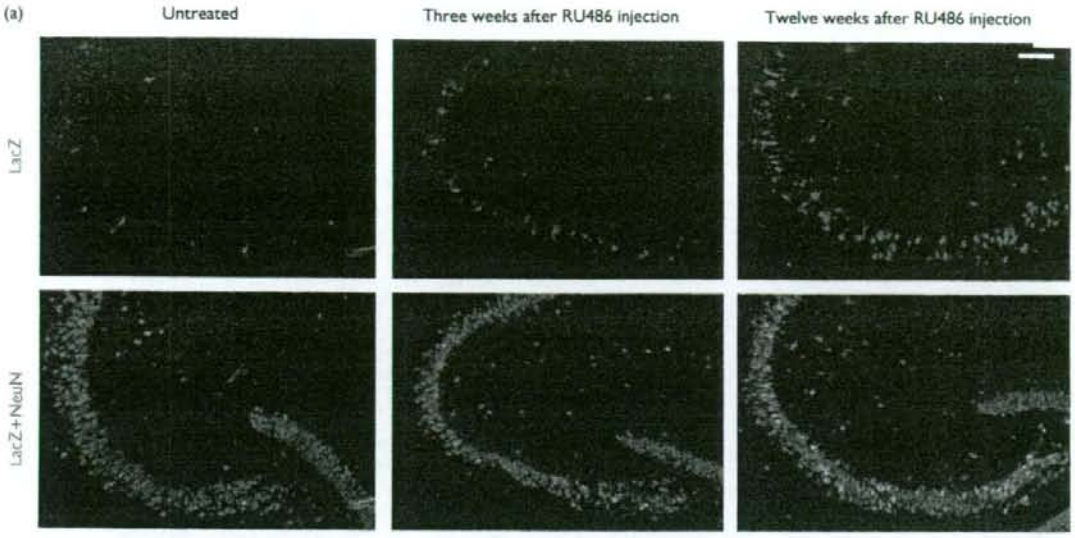

(b)

	LacZ positive cells/NeuN positive cells (%)
Untreated	1.5
Three weeks after RU486 injection	6.0
Twelve weeks after RU486 injection	17.3

Fig. 2 Immunohistochemical analysis of recombinase activity induced by RU486. (a) Sections of the hippocampus were double-stained with anti-lacZ antibody (green) (top panels) and anti-NeuN antibody (marker of neurons; red) (merge; bottom panels). Samples were obtained from $\tau^{CrePR}/+$; *R26R*/+ mice without RU486 injection (left panels) and 3 and 12 weeks after intraperitoneal RU486 injection (middle and right panels, respectively). Scale bar, 100 μm. (b) Induction ratio of Cre recombinase activity (percentage of LacZ-positive neurons) by RU486 in CA3 regions of the hippocampus. CrePR, Cre recombinase and the progesterone receptor; NeuN, neuronal nuclei.

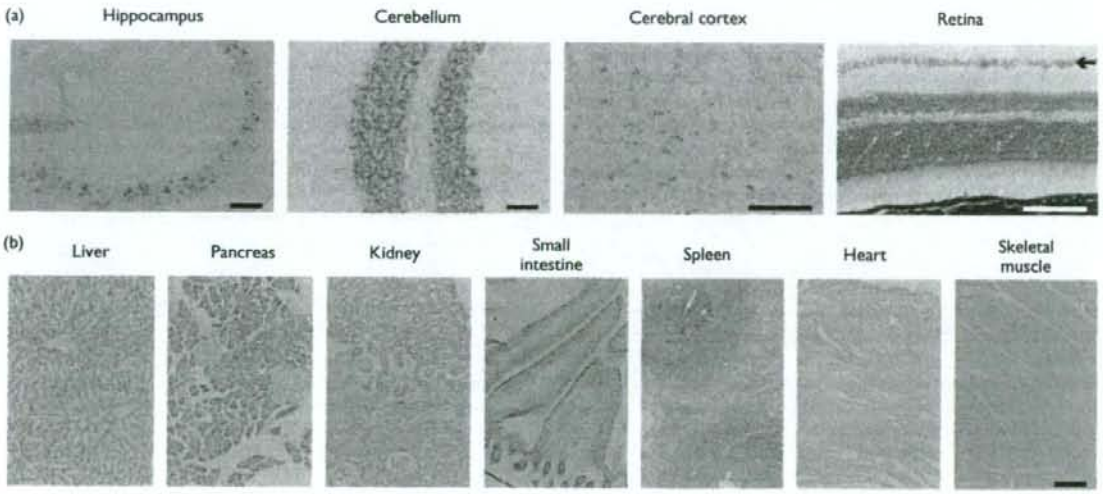

Fig. 3 Neuron-specific induction of Cre-mediated excision in $\tau^{CrePR}/+$; *R26R*/+ mice by RU486 injection. (a) LacZ-stained frozen sections in $\tau^{CrePR}/+$; *R26R*/+ mice 12 weeks after RU486 injection. Staining is discernible in neurons in the hippocampus, cerebral cortex, cerebellum, and retina. The arrow shows the layer of ganglion cells. Scale bars, 100 μm. (b) No lacZ activity was detected in tissues other than the nervous system. Scale bar, 100 μm for all panels. CrePR, Cre recombinase and the progesterone receptor.

Neuron-specific recombination induced by RU486 injection

To examine the recombinase activity of the CrePR induced by antiprogesterone RU486, τ^{CrePR} were crossed with *Gt (ROSA)*^{26Sor} *lacZ* reporter mice (*R26R* mice) [13]. In *R26R* mice, Cre-mediated excision of a floxed cassette results in LacZ expression, which can be detected as β-gal activity (Fig. 1a).

The offspring containing each of the mutant gene heterozygously (τ^{CrePR}/+; *R26R*/+) were used to evaluate CrePR activity. RU486 was injected intraperitoneally into τ^{CrePR}; *R26R* double heterozygous mice 1 mg/g/day for 2 consecutive days. We compared the expression of β-gal in mice 3–12 weeks after RU486 injection to the expression of β-gal in untreated mice. Immunostaining revealed that neuron-specific recombination was induced in a time-dependent manner in the hippocampus (Fig. 2). In CA3 region of the hippocampus, 17.3% of the neurons were stained by the anti-LacZ antibody 12 weeks after RU486 injection, whereas only 1.5% of the neurons were stained in the untreated mouse. Similar neuron-specific and time-dependent recombination was also induced in other regions of the nervous system (data not shown).

X-gal staining revealed that the expression of β-gal was limited to neurons and was not detected in glias and other tissues in τ^{CrePR}; *R26R* double heterozygous mice. After RU486 injection, β-gal was detected in neurons in the hippocampus and the cerebral cortex, Purkinje cells in the cerebellum and ganglion cells in the retina (Fig. 3a). In contrast, we detected no recombination in the other tissues including the liver, kidney, and intestine (Fig. 3b).

Discussion

To establish neuron-specific and inducible gene targeting system, we have generated the τ^{CrePR} knockin mice. In τ^{CrePR} mice, we observed inducible recombination by Cre recombinase in the cerebral cortex, hippocampus, cerebellum, and retina. Although several protocols of RU486 administration were applied, the Cre recombination ratios were not as high as expected. The recombination ratio is even lower than that reported in earlier studies. For instance, earlier studies reported that the recombination efficiency after RU486 administration was 50–70% in the hippocampus [6], 90% in cerebellar granule cells [8], and 80–90% in cerebellar Purkinje cells [10]. The low recombination efficiency in our mice may be due to the low delivery efficiency of RU486 to the brain or low recombination efficiency by CrePR fusion proteins.

In CrePR/loxP system, background recombinase activity seemed to be higher than that of CreER^{T}/loxP system [6,14]. Our data also showed there was a low but detectable recombination in neurons without induction as reported previously [8,15]. Although this background activity and low recombination efficiency should be improved, we believe that the τ^{CrePR} knockin line will be a useful tool for various genetic analysis of neuronal functions. For example, low recombination efficiency would allow the knockout mice to live long enough to examine the function of the gene of interest, even if the gene is essential for neuronal function. It also allows one to compare the neurons deficient in the targeted gene and the surrounding normal neurons ('mosaic analysis'). Thus, τ^{CrePR} mice would see applications in studying the functions of genes involved in neuronal development, maintenance and degeneration.

Conclusion

We have generated the neuron-specific and inducible mouse line using CrePR/loxP system. The efficiency and specificity of the τ^{CrePR} knockin line suggest that the line is a useful tool for the genetic analysis of neuronal functions.

Acknowledgements

The authors acknowledge Professor K. Sakimura for technical advice. The authors also thank Mses. M. Takano, T. Horie, and Y. Okada for their technical assistance. This study was supported by Grants-in-Aid for scientific research from the Ministry of Education, Culture, Sports, Science and Technology of Japan (MEXT), Initiatives for Attractive Education in Graduate Schools from MEXT, and the grant from Fumi Yamamura Memorial Foundation for Female Natural Scientists.

References

1. Tronche F, Kellendonk C, Kretz O, Gass P, Anlag K, Orban PC, *et al.* Disruption of the glucocorticoid receptor gene in the nervous system results in reduced anxiety. *Nat Genet* 1999; **23**:99–103.
2. Hirasawa M, Cho A, Sreenath T, Sauer B, Julien JP, Kulkarni AB. Neuron-specific expression of Cre recombinase during the late phase of brain development. *Neurosci Res* 2001; **40**:125–132.
3. Zhu Y, Romero MI, Ghosh P, Ye Z, Charnay P, Rushing EJ, *et al.* Ablation of NF1 function in neurons induces abnormal development of cerebral cortex and reactive gliosis in the brain. *Genes Dev* 2001; **15**: 859–876.
4. Metzger D, Clifford J, Chiba H, Chambon P. Conditional site-specific recombination in mammalian cells using a ligand-dependent chimeric Cre recombinase. *Proc Natl Acad Sci U S A* 1995; **92**:6991–6995.
5. Kellendonk C, Troche F, Monaghan AP, Angrand PO, Stewart F, Schutz G. Regulation of Cre recombinase activity by the synthetic steroid RU486. *Nucleic Acids Res* 1996; **24**:1404–1411.
6. Kellendonk C, Tronche F, Casanova E, Anlag K, Opherk C, Schutz G. Inducible site-specific recombination in the brain. *J Mol Biol* 1999; **285**:175–182.
7. Vegeto E, Allan GF, Schrader WT, Tsai MJ, McDonnell DP, O'Malley BW. The mechanism of RU486 antagonism is dependent on the conformation of the carboxy-terminal tail of human progesterone receptor. *Cell* 1992; **69**:703–713.
8. Tsujita M, Mori H, Watanabe M, Suzuki M, Miyazaki J, Mishina M. Cerebellar granule cell-specific and inducible expression of Cre recombinase in the mouse. *J Neurosci* 1999; **19**:10318–10323.
9. Takeuchi T, Miyazaki T, Watanabe M, Mori H, Sakimura K, Mishina M. Control of synaptic connection by glutamate receptor δ2 in the adult cerebellum. *J Neurosci* 2005; **25**:2146–2156.
10. Kitayama K, Abe M, Kakizaki T, Honma D, Natsume R, Fukaya M, *et al.* Purkinje cell-specific and inducible gene recombination system generated from C57BL/6 mouse ES cells. *Biochem Biophys Res Commun* 2001; **281**: 1134–1140.
11. Harada A, Oguchi K, Okabe S, Kuno J, Terada S, Ohshima T, *et al.* Altered microtubule organization in small-calibre axons of mice lacking tau protein. *Nature* 1994; **369**:488–491.
12. Harada A, Sobue K, Hirokawa N. Developmental changes of synapsin I subcellular localization in rat cerebellar neurons. *Cell Struct Funct* 1990; **15**:329–342.
13. Soriano P. Generalized lacZ expression with the ROSA26 Cre reporter strain. *Nat Genet* 1999; **21**:70–71.
14. Brocard J, Warot X, Wending O, Messaddeq N, Vonesch JL, Chambon P, *et al.* Spatio-temporally controlled site-specific somatic mutagenesis in the mouse. *Proc Natl Acad Sci U S A* 1997; **94**:14559–14563.
15. Kyrkanides S, Miller J, Bowers WJ, Federoff HJ. Transcriptional and posttranslational regulation of Cre recombinase by RU486 as the basis for an enhanced inducible expression system. *Mol Ther* 2003; **8**: 790–795.